The Human Hippocampus Is Involved in Auditory Short-Term Memory Trace Formation

Xiuyuan Liang[1,4,5,†], Zihao Guo[1,†], Dong Zhang[2], Yiming Zhang[2], Aobo Chen[2], Lanlan Wang[3], Xiang Liu[3], Wang Zhang[2], Yinbao Qi[2], Xiaorui Fei[2], , Ming Wang[1], Huawei Li[6], Lin Chen[1,6,*], Ruobing Qian[2,*]

[1]Auditory Research Laboratory, School of Life Sciences, Division of Life Sciences and Medicine, University of Science and Technology of China, Hefei 230027, China

[2]Department of Neurosurgery, The First Affiliated Hospital, Division of Life Sciences and Medicine, University of Science and Technology of China, Hefei 230001, China

[3]Department of Neuroelectrophysiology, The First Affiliated Hospital, Division of Life Sciences and Medicine, University of Science and Technology of China, Hefei 230001, China

[4]National Engineering Research Center of Speech and Language Information Processing, University of Science and Technology of China, Hefei 230027, China

[5]Interdisciplinary Research Center for Linguistic Sciences, School of Humanities and Social Sciences, University of Science and Technology of China, Hefei 230027, China

[6]Affiliated Eye and ENT Hospital of Fudan University, Shanghai 200031, China

[†]These authors contributed equally to this work.

*Correspondence to: Lin Chen

Full address: Auditory Research Laboratory, School of Life Sciences, Division of Life Sciences and Medicine,University of Science and Technology of China, Hefei 230027, China

E-mail: linchen@ustc.edu.cn

*Correspondence to: Ruobing Qian

E-mail: qianruobing@ustc.edu.cn

Full address: Department of Neurosurgery, The First Affiliated Hospital, University of Science and Technology of China, Hefei 230001, China

Abstract

The human hippocampus has been claimed to play an important role in long-term memory, or episodic memory. It has long been argued whether the hippocampus does contribute to short-term memory. Here, we demonstrate human hippocampus has been involved in auditory short-term memory (ASTM) trace formation. We used a classic oddball paradigm and intracranial recordings across various human brain areas. High frequency activities evoked by deviant stimuli in subjects indicate the generation of ASTM trace. Auditory response latencies recorded from the hippocampus, insula, temporal lobe, parietal lobe, and frontal lobe showed the early processing of ASTM trace at a pre-attention stage. Moreover, Granger causality analyses showed ASTM trace is processed in hierarchical cortical areas and interactions among this memory process have been clarified. Specifically, bottom-up auditory signals processed by the insula, and auditory regions of the temporal lobe and the frontal lobe at an early stage, then auditory top-down information transmitted from the frontal lobe to the hippocampus, the inferior temporal lobe, as well as insula at a relatively late pre-attention stage of the auditory information processing. These results provide evidence that the human hippocampus contributes to the short-term memory of auditory perception at a pre-attention stage and suggests a challenge to entrenched beliefs in the classification/definition of memory systems.

Keywords: auditory short-term memory trace; hippocampus; stereoencephalography (sEEG); high-frequency activity (HFA)

Introduction

The human hippocampus has been claimed to play a crucial role in human memory system especially long-term memory, also referred to as episodic memory[1], it comes with an equally important caveat that the hippocampus does not contribute to short-term memory[2]. The traditional/conventional view of hippocampal amnesia is that short-term memory is preserved despite the severe impairment in long-term memory[1,3,4]. For several years, a wide range of studies have established the medial temporal lobe, and hippocampus in particular, to be critically associated with long-term memory processing. For instance, researchers studied H.M., the well-known amnesic patient who had undergone temporal lobe resection, and published observations of some types of preserved memory (motor skill and perceptual learning) in the patient[5,6], as well as types of memory that depended on parts of the brain

other than the medial temporal lobe, in particular the hippocampus, or that did not depend on conscious awareness were termed implicit (non-declarative) memory[7,8]. Previous view mentioned that amnesia associated with hippocampal region damage is selective to declarative memory, the ability to recall facts and events[9], and for H.M. the deficit includes the complete absence of episodic memory, defined as the ability to remember specific personal experiences[10]. In addition, many researchers have explored the underlying neural mechanism of memory in which studies have implied that selective injury to the medial temporal lobe leads to an isolated deficit in long-term memory[11,12]. Evidence from studies in patients with amnesia due to hippocampal damage proposed that patients exhibit impairment of conscious episodic encoding and retrieval[13]. Nevertheless, there is different view reports that amnesic patients with bilateral lesions involving the hippocampus region suffered from an impairment of short-term memory along with research develops[14,15]. Moreover, recent visual study in human supports the view that the hippocampus does indeed have a role to play in short-term memory[16] and study reported the role of cross-frequency coupling in cortico-hippocampal activity in sequential auditory short-term memory (ASTM)[17].

Short-term memory is a storage system that has an evolutionary survival advantage, such as paying attention to limited but essential information excluding confounding factors and ASTM is one of the important sensory-associated subsystems[18]. Short-term memory trace is the physical neural basis for that function—the temporary, biological activity in our brain that makes short-term memory possible. Mismatch negativity (MMN), the index of automatic deviance detection, reflects the cortical responses to deviant changes occurred in the auditory system[19,20], has been regarded as the detection of a deviant stimulus within the ASTM[21], was first described about 40 years ago by Näätänen and his colleagues[22]. A various of studies leading to believe that the MMN is the outcome of an automatic comparison process between a new, deviant stimulus and the memory trace formed by the sensory representation of the standard stimuli within the short-term memory[23-26]. The MMN depends on the presence of a ASTM trace in the auditory cortex representing the repetitive aspects of the preceding auditory events[19]. Thus, ASTM trace formation is indexed by the MMN responses and deviance detection is mediated by a more stable short-term memory trace[27,28]. In the current study, we used a short-term memory paradigm presented with a contrast auditory stream created by different pure tones and intracranial recordings, a high spatial and temporal resolution electrophysiological study across various human brain regions to explore whether the human hippocampus contributes to/is involved in ASTM trace formation process.

High frequency activities (HFA, 70–150 Hz) elicited by the auditory stimuli is a reliable electrophysiological correlate of underlying averaged spiking activity generated by the thousands of neurons that are in the immediate vicinity of the recording electrodes[29-32]. This type of activity has been linked to various cognitive processes, including attention, memory, and sensory processing. Significant HFA of deviance detection evoked by the subjects indicate the generation of ASTM trace. In our study, HFA results revealed that hippocampus was involved during process of ASTM trace. Auditory response latencies recorded from the hippocampus, insula, temporal lobe, parietal lobe, and frontal lobe showed the early processing of ASTM trace at a pre-attention stage. Moreover, Granger causality analysis further demonstrated ASTM trace is processed in hierarchical cortical areas, and detailed interactions of brain regions among this memory trace process have been clarified/interpreted clearly. Specifically, bottom-up auditory signals processed by the insula, and auditory regions of the temporal lobe and the frontal lobe at an early stage, then auditory top-down information transmitted from the frontal lobe to the hippocampus, the inferior temporal lobe, as well as insula at a relatively late pre-attention stage of the auditory information processing. To sum up, these results provide evidence that the human hippocampus contributes to the ASTM trace of auditory perception at a pre-attention stage. Accompanied by the specific hierarchical network of deviance processing obtained from Granger causal analysis, the current study presents a more comprehensive and detailed understanding the formation of ASTM trace, suggests a challenge to entrenched beliefs in the classification/definition of memory systems.

Materials and methods

Ethics statement

This study was approved by the Research Ethics Committee of the First Affiliated Hospital, University of Science and Technology of China. All participants provided written informed consent prior to taking part in the study. Neither the study procedures nor the analytical methods were preregistered in a time-stamped institutional registry before the research was conducted.

Participants

Stereoelectroencephalography (sEEG) data were obtained from 17 patients (6 males, 11 females) with drug-resistant epilepsy who were being evaluated as potential candidates for resective surgery. Data collection took place at the First Affiliated Hospital, University of Science and Technology of China. As part of their presurgical assessment, each patient underwent invasive sEEG monitoring. The selection of regions for electrode implantation was determined solely by clinical criteria. All participants were implanted with intracranial depth sEEG electrodes (0.8 mm in diameter, with a 3.5 mm center-to-center interelectrode distance) to help localize the epileptogenic zone. Every participant was right-handed, had normal cognitive function, and normal hearing. Written informed consent was obtained from all subjects prior to enrollment. The experimental protocol received approval from the Institutional Review Board of the University of Science and Technology of China and the First Affiliated Hospital.

Task paradigm

Stimuli in the current study consisted of pure tones generated using Audition 3.0 (Adobe Systems Inc., Mountain View, CA, USA). The auditory contrast was formed by a sequence of 300 ms pure tones, with a 500 Hz tone serving as the frequent standard stimulus and a 700 Hz tone as the infrequent deviant stimulus (**Figure 1**). All stimuli were delivered in random order via headphones using E-Prime (Psychology Software Tools, Inc., USA). Participants were instructed to ignore the auditory stimuli and instead focus on watching a muted movie of their choice with subtitles.

Data acquisition

For each participant, structural MRI scans were acquired prior to electrode implantation, and post-implantation CT scans were obtained afterward. sEEG signals were recorded using a 128/256-channel Neurofax EEG-1200c amplifier/digitizer system (Nihon Kohden, Japan) via implanted depth electrodes. Recording settings included a high-pass filter with a 0.01 Hz cut off, a 50 Hz notch filter, and a sampling rate of either 2000 Hz or 5000 Hz. Electrodes located on the inner surface of the skull served as the ground and reference.

Preprocessing and Electrode localization

Our sEEG data was imported to MATLAB using FieldTrip toolbox[33] and resampled to 1000 Hz. Event onset markers were read from pre-allocated trigger channels. The data were then re-referenced to the mean of the mastoid electrodes, and unused channels were removed. Segments containing epileptiform activity or abnormal fluctuations were manually rejected. The electrode localization was based on the FieldTrip protocol[34] with an adaptation for Windows, in which post-implantation CT images was co-registered to pre-implantation MRI images using SPM 12[35]. The images were subsequently normalized to the MNI-152 template space using SPM12[36], and electrode positions were determined according to the FieldTrip pipeline.

High frequency activity (HFA) analysis

Line noises at 50 Hz, 100 Hz, and 150 Hz was removed using a notch filter. The continuous data were segmented into 900 ms epochs (□200 ms to 700 ms). Trials were rejected if the amplitude exceeded 5 SD standard deviations from the mean for more than 25 consecutive ms, or if the power spectral density exceeded 5 standard deviations for more than 6 consecutive Hz[37]. Eligible trials were re-referenced to a neighboring channel for HFA analysis. HFA signals from –100 ms to 600 ms were extracted for further processing. Preprocessed data were band-pass filtered into eight 10-Hz-wide bands ranging from 70 to 150 Hz using a zero-phase Hamming windowed FIR filters (order 138)[38]. The envelope of each narrowband signal was extracted by taking the absolute value of the analytic signal from the Hilbert transform, and each amplitude time series was divided by its mean value[39]. For channels exhibiting a significant linear trend (R-square > 0.3), the trend was removed. Each channel's baseline period was removed and normalized by dividing the standard deviants of all trials of the baseline period.

Tone response and deviance detection

To identify channels with significant responses to auditory stimuli, a two-tailed cluster-based permutation test with threshold-free cluster enhancement[40] and 1000 sign-flipping randomizations[41] was applied separately to standard and deviant trials for each channel. Channels with a corrected p-value below 0.05 either stimulus type were considered responsive. Channels displaying abnormal waveforms or epileptic activity were subsequently excluded through manual review. Then, in order to assess whether a channel was involved in deviance detection, a two-tailed cluster-based permutation test with threshold-free cluster enhancement[40] and 1000 randomizations was applied to compare trial categories (standard vs. deviant) for each channel. Channels with a corrected p-value less than 0.05 were considered significant for deviance detection. Additional manual rejection was applied to exclude channels with aberrant signals or association with epileptic activity. The latency of high-frequency activity (HFA) responses was estimated using a fractional area method[42]. The procedure began by identifying the time point of maximum amplitude within the response window as the initial seed point. The significant cluster was expanded bilaterally from this seed until the amplitude dropped below 20% of the seed value or reached the epoch boundaries. The latency was defined as the center of mass of the resulting suprathreshold cluster.

Event-related potential analysis and clustering

Event-related potentials (ERP) were derived from the same trials used in the high-frequency activity (HFA) analysis, prior to re-referencing to neighboring channels. The ERP signals were filtered with a zero-phase FIR filter (order 18, 1–20Hz), segmented into 700 ms epoches (–100 ms to 600 ms relative to stimulus onset) and baseline-corrected by subtracting the mean amplitude during the –100 ms to 0 ms interval. For channels exhibiting a significant linear trend (R-square > 0.3), detrending was applied. Similar to the HFA analysis, a two-tailed cluster-based permutation test incorporating threshold-free cluster enhancement (TFCE) was conducted for each electrode shaft to identify channels with significant responses to deviant stimuli. Using principal component analysis (PCA) in line with Blenkmann et al.[37], we identified groups of event-related potential (ERP) responses exhibiting consistent temporal patterns across channels and subjects. This approach also enabled the mitigation of polarity reversal effects. The analysis proceeded as follows: first, a difference waveform was computed by subtracting the standard stimulus response from the

deviant stimulus response. PCA was then applied to this difference signal, and the first four components capturing the highest channel weights were retained. Channels were grouped based on their highest component weight, those predominately weighted on the first component were clustered together, followed by those associated with the second component, and so forth for each subsequent component.

Granger Causality Analysis

Wiener-Granger causality (G-causality, GC) is a statistical notion of causality applicable to time series data, whereby cause precedes, and helps with prediction[43,44], which has been developed to a powerful method for identifying information transfer or directed functional ("causal") connectivity in neural time series data[45,46]. It is defined in both time and frequency domains, and allows for the conditioning out of common causal influences. Originally developed in the context of econometric theory, it has since achieved broad application in the neurosciences and beyond[47]. G-causality says that a variable X "G-causes" another variable Y if the past of X contains information that helps predict the future of Y, over and above the information already in the past of Y itself (and in the past of other "conditioning" variables Z). In general terms, when this condition is satisfied one can say that there is "information flow" from X to Y. This is justified because G-causality is an approximation to transfer entropy (the approximation is exact for Gaussian variables), which is a directed version of Shannon's mutual information, a very general way of characterizing the statistical dependency or shared information between two variables[48]. The multivariate Granger causality analysis (MVGC) Matlab toolbox used in the current study was designed for applications in neuroscience[49], which implements numerical routines for calculating multivariate Granger causality (MVGC) from time series data, both unconditional and conditional, in the time and frequency domains[50]. Since it has been recognized that a moving average (MA) component in the data presents a serious confound to Granger causal analysis, as routinely performed via autoregressive (AR) modeling[49]. Previous studies have solved this problem by demonstrating that Granger causality may be calculated simply and efficiently from the parameters of a state-space (SS) model[44]. Because SS models are equivalent to autoregressive moving average models, Granger causality estimated in this fashion is not degraded by the presence of a MA component. State-space Granger causal inference stands to significantly enhance our ability to identify and understand causal interactions and information flow in the current study[51]. We used the MVGC (Multivariate Granger Causality) Matlab toolbox for calculating multivariate Granger causality from time series

data[49]. Autoregressive moving average (ARMA) process or, equivalently, finite order linear state-space (SS) have been applied in this study[51]. We selected a time window of interest spanning –100 ms to 600 ms to perform identical analyses. The model order was estimated using Akaike information criterion. The significance of difference of G-causality between standard and deviant conditions was estimated using a permutation test.

Results

The hippocampus exhibited a significant high-frequency activity (HFA) response during auditory deviance detection.

In the current study, we employed a classic auditory oddball paradigm combined with intracranial recordings across multiple human brain regions to investigate the neural mechanisms underlying short-term memory trace formation. The hippocampus, a key structure within the medial temporal lobe memory system, is critically involved in the integration and relay of auditory information to downstream perceptual and cognitive regions[52-55]. Thus, for each recording channel in the hippocampal region, we computed trial-averaged high-frequency activity responses to both standard and deviant pure tones (Fig. 2).

Our results revealed that hippocampal channels displayed diverse response profiles, including both HFA enhancements and high-frequency suppression (HFS). Specifically, responses to standard stimuli were predominantly characterized by negative-going deflections (Fig. 2a and Fig. 2c), whereas responses to deviant stimuli consistently exhibited positive deflections (Fig. 2e and Fig. 2g). To identify channels exhibiting significant responses to auditory stimuli, a two-tailed cluster-based permutation test incorporating threshold-free cluster enhancement (TFCE)[40] was applied separately to standard and deviant trials for each channel. The test was performed using 1000 sign-flipping randomizations. Channels with a corrected p-value below 0.05 for either stimulus type were classified as responsive. Exemplar channels exhibiting statistically significant responses to standard pure tones are shown in or deviant pure tones are shown in Fig. 2b and Fig. 2d ($p < 0.05$), while exemplar channels exhibiting statistically significant responses to deviant pure tones are presented in Fig. 2f and Fig. 2h ($p < 0.05$).

Classifications of High-Frequency Responses to Pure Tones.

Furthermore, electrode pairs that evoked significant mismatched activity were categorized according to whether the mismatch activity was enhanced or suppressed. We collected sEEG data from 17 epilepsy patients (Table 1). To obtain a global description of the brain regions in deviance detection, we examined the HFA responses to standard versus deviant tones across intracranial channels. In the HFA analysis, 49 channels responded to tone responses in 10 out of the 17 patients (Fig. 3), which illustrates the overall response profiles across all channels, including both HFA and high-frequency suppression (HFS). Specifically, Significant HFS responses were observed in 8 channels across 6 patients with and 41 channels across 10 subjects with HFA responses ($p < 0.05$, Fig. 3a, b). HFS in response to the stimuli at a latency of 395 ms were recognized at the middle temporal gyrus (MTG), temporo-occipital brain area, posterior inferior temporal gyrus, and anterior corona radiata a channel. In addition, 29 channels across 9 patients responded exclusively to deviant stimuli (Fig. 3c) whereas 12 channels across 7 patients responded to both standard and deviant tones (Fig. 3d). It is known that studying HFA with sEEG recordings can provide insights into the neural bases of human cognition that cannot be derived as easily from the study of BOLD effects with fMRI or from the analysis of EEG[30]. HFS, a transient energy suppression in the gamma-band (40–150 Hz) during the processing of sensory stimuli, which was first reported by Lachaux[56] and has close relationship with attention[57]. We also observed widely distributed high frequency suppression (HFS)[58], particularly in response to standard stimuli, which generally occurred later than high frequency activity (HFA). This widespread HFS may reflect an energy saving mechanism in the brain when processing predictable events. Given the known interaction between early tone responses and later repetition suppression[59], such suppression may be mediated by repetition suppression mechanisms. Supplementary Figure 1 showed HFA responses across individual patients.

Various brain regions showed significant HFA during short-term memory trace formation.

We investigated the spatiotemporal dynamics and effective connectivity of high-frequency activity (HFA) responses across key brain regions during the processing of auditory deviant stimuli (Fig S1). Mean HFA/HFS responses to standard and deviant pure tones, along with the deviant-minus-standard difference waveforms were shown for multiple brain regions (Fig. 4a). These brain regions included the insula; temporal lobe (encompassing Heschl's

gyrus, superior temporal gyrus, and superior temporal sulcus); frontal lobe (including the middle frontal gyrus, superior frontal gyrus, anterior cingulate cortex, and frontal operculum); parietal lobe (comprising the postcentral gyrus, parietal operculum, and supramarginal gyrus); posterior temporal lobe (the temporo-occipital part of the middle temporal gyrus); inferior temporal lobe (including the inferior temporal gyrus, fusiform gyrus, and inferior portion of the middle temporal gyrus); and the hippocampal area (encompassing the hippocampus, parahippocampal gyrus, and amygdala). Moreover, A scatter plot illustrates the response latencies of HFA/HFS from electrode pairs in the aforementioned regions. The data reveal a systematic, ascending trend in response latencies across these different brain areas (Fig. 4b), suggesting a sequential propagation of deviance processing. Brain regions included the insula, temporal lobe (i.e., Heschl's gyrus, STG, superior temporal sulcus, STS), frontal lobe (inferior frontal gyrus middle frontal gyrus, anterior (para) cingulate cortex, frontal operculum), parietal lobe (parietal lobe postcentral gyrus, central opercular cortex, parietal operculum, supramarginal gyrus), posterior temporal lobe (temporooccipital division) hippocampus, and the inferior temporal lobe (fusiform gyrus, inferior temporal gyrus, middle temporal gyrus) were all involved during the processing of deviance detection, and the latencies of auditory mismatch HFA of these brain areas ranged from 110 ms to 438 ms (Fig. 4b).

Granger causality analysis showed connectivity of the hippocampus with various brain regions.

Next, we investigated the neural connectivity underlying auditory deviance processing by applying linear Granger causality analysis. To effectively visualize the complex network, electrode pairs were first merged according to their respective brain regions. The analyzed regions included the insula; temporal lobe (Heschl's gyrus, superior temporal gyrus, superior temporal sulcus); frontal lobe (middle frontal gyrus, superior frontal gyrus, anterior cingulate cortex, frontal operculum); parietal lobe (postcentral gyrus, parietal operculum, supramarginal gyrus); posterior temporal lobe (temporo-occipital part of the middle temporal gyrus); inferior temporal lobe (inferior temporal gyrus, fusiform gyrus, inferior portion of the middle temporal gyrus); and the hippocampal area (hippocampus, parahippocampal gyrus, amygdala). The anatomical locations of these regions were mapped onto a common cortical space, as shown in the enlarged image of the boxed area, with different colors denoting

distinct brain clusters. The resulting connectivity is depicted in the heatmap (Fig. 4c), which displays the estimated difference in Granger causal connection strengths between deviant and standard stimulus-evoked activities. Each cell represents the strength of the causal influence from the row-specified region to the column-specified region. Gray indicates connections with no significant difference between conditions, whereas colored cells represent pathways where the deviant stimulus elicited a significant change in effective connectivity. The brain regions implicated by Granger causality analysis were rendered on a standardized cortical surface. A magnified inset of the demarcated area is presented, in which unique colors code for separate functional clusters and the directionality (bottom-up versus top-down) of their causal influences (Fig. 5).

Intracranial event-related potentials

Mean event-related potential (ERP) responses to standard and deviant pure tones, as well as the deviant-minus-standard difference waveforms were analyzed. Fig S2 showed ERP responses across individual patients. To ensure waveform comparability, only channels exhibiting significant responses to both conditions within each analytical dimension were included in the averages and subsequent plots. The induced activity in the high gamma band as mismatch response (MMR), an intracranial EEG counterpart to scalp mismatch negativity (MMN)[60]. Given that the same neural phenomenon can be recorded either as a positive or a negative intracranial ERP (iERP)[30]. An iERP equivalent to the scalp mismatch response were shown in Fig S3. And iERP effects were present in 188 channels across 17 patients. Cause we grouped the iERP responses from different channels according to the highest weights of the PCA decomposition. Figure 4 shows the iERP responses to deviant and standard tones for the four groups of channels. Differences in Group 1 (n = 121, s = 6), group 2 (n = 41, s= 6) and group 4 (n = 8, s = 4) showed significant MMR ($P < 0.05$), and differences in group 3 (n = 18, s = 3) showed significant MMN ($P < 0.05$).

Discussion

In the current study, we employed a short-term memory paradigm featuring a contrastive auditory stream of pure tones to investigate the role of the human hippocampus in the formation of auditory short-term memory (ASTM) trace. Combined with high spatiotemporal

resolution approach, intracranial recordings used in this study allowed us to examine the electrophysiological activity across multiple brain regions. High-frequency activity (HFA, 70–150 Hz), a reliable electrophysiological correlate of localized neuronal firing, served as our primary metric. The significant HFA elicited during deviance detection indicates the generation of ASTM trace. Our results revealed that the hippocampus is involved in this process. Furthermore, the response latencies observed in the hippocampus, insula, temporal, parietal, and the frontal regions suggest that the initial process of the ASTM trace occurs at a pre-attention stage. Furthermore, Granger causality analysis demonstrate that the ASTM trace is processed through a hierarchical cortical network. Specifically, bottom-up auditory signals were initially processed by the insula and auditory regions of the temporal and frontal regions. This was followed by the top-down information flow from the frontal region to the hippocampus, inferior temporal lobe, and insula at a later pre-attention stage. In summary, these findings provide direct evidence that the human hippocampus contributes to ASTM trace formation at a pre-attention stage. Coupled with the specific hierarchical network for deviance processing identified through Granger causality, our study offers a more comprehensive model of ASTM trace formation and challenges entrenched definition of memory systems.

The hippocampus is involved in processing of auditory short-term memory trace formation.

The hippocampus is well known to be involved in the medial temporal lobe memory system and also has been thought to play a critical role in relaying auditory information to later perceptual and cognitive processes[52-55]. In terms of auditory perception, the hippocampus receives afferent inputs form the auditory association cortices, and in turn, it projects back to the primary auditory cortex and auditory association areas[61,62]. MRI and MEG recordings combined with equivalent current dipole (ECD) analysis revealed electrophysiological signatures of hippocampal involvement in auditory processing[62]. The noise responses of hippocampal neurons in awake mice have identified a population of neurons that can be associated with auditory fear conditioning[63]. Previous study used ERPs and event-related magnetic fields (ERFs) to investigate the relationship between the hippocampus and the event-related responses in auditory information processing[64]. Results have suggested that the auditory processing is carried out by the combination of multiple structures including the

mesial temporal area, the superior temporal area and the inferior parietal area on both hemispheres, and that the generator (hippocampus) in the mesial temporal area contributes to the scalp-recorded P300 only at the corresponding anterior temporal region[64]. MEG and effective connectivity analyses (dynamic causal modeling) showed that the hippocampus and ventromedial prefrontal cortex (vmPFC) work as a functional circuit during mismatch detection, suggesting that the vmPFC drives the hippocampus during the generation and processing of mismatch signals[65]. Previous intracranial and lesion research proposed that hippocampus is involved with novelty processing in a fronto-hippocampal network and the hippocampus plays an active role in contextual updating at the end of the cognitive episode[66].

In terms of auditory perception, the hippocampus receives afferent inputs form the auditory association cortices, and in turn, it projects back to the primary auditory cortex and auditory association areas[61,62]. MRI and MEG recordings combined with equivalent current dipole (ECD) analysis revealed electrophysiological signatures of hippocampal involvement in auditory processing[62]. The noise responses of hippocampal neurons in awake mice have identified a population of neurons that can be associated with auditory fear conditioning[63]. Previous study used ERPs and event-related magnetic fields (ERFs) to investigate the relationship between the hippocampus and the event-related responses in auditory information processing[64]. Results have suggested that the auditory processing is carried out by the combination of multiple structures including the mesial temporal area, the superior temporal area and the inferior parietal area on both hemispheres, and that the generator (hippocampus) in the mesial temporal area contributes to the scalp-recorded P300 only at the corresponding anterior temporal region[64].

Auditory short-term memory trace is processed in hierarchical cortical areas.

Predictive coding theories posit that neural networks learn statistical regularities in the environment for comparison with actual outcomes, signaling a prediction error (PE) when sensory deviation occurs[67]. The predictive coding model of perception proposes that neuronal responses are modulated by the amount of sensory input that the internal prediction cannot account for (i.e., prediction error) and postulates that perception entails the top-down propagation of prediction and the bottom-up propagation of prediction error[68]. Within a predictive coding framework, MMN and novelty-related ERP signatures are interpreted as

prediction-error responses that signal the mismatch between sensory inputs and internal models[69]. The MMN is considered the classic PE signal elicited during passive listening to deviant sounds interrupting the context provided by a sequence of repeated standard stimuli[70]. Auditory prediction errors, i.e. the mismatch between predicted, forthcoming auditory sensations and actual sensory input, trigger the detection of surprising auditory events in the environment (Friston, 2005). Previous studies used DCM to investigate the effective connectivity of auditory mismatch responses and demonstrated a three-level hierarchical network comprised of connections from bilateral primary auditory cortex (A1) to the planum temporale (PT), and from the PT to the right inferior frontal gyrus (IFG) (Garrido et al., 2007, 2008). This network included intrinsic (within source) connections in A1 and extrinsic (between-sources), forward and backward, connections between A1, PT and IFG. The signaling of top-down (feedback signals) predictions and bottom-up (feedforward signal) prediction errors conveyed across hierarchical regions[71].

The formation of the ASTM trace is not an isolated function of a single region but arises from coordinated activity within a hierarchical cortical network. Our Granger causality analysis, based on a state-space model, delineated the specific directional information flows underlying this process. The network operates through a dynamic interplay of bottom-up and top-down processing. Bottom-up auditory signals from the deviant stimulus are initially processed by the insula and auditory regions within the temporal and frontal lobes. Subsequently, at a later pre-attention stage, a top-down information flow emerges from the frontal region back to the hippocampus, inferior temporal lobe, and insula. This connectivity pattern positions the hippocampus within a regulated circuit. The hippocampus appears to be driven by higher-order frontal regions during the processing of mismatch signals. This is consistent with previous effective connectivity analyses (e.g., Dynamic Causal Modeling) showing that structures like the ventromedial prefrontal cortex (vmPFC) drive the hippocampus during mismatch detection[65]. Furthermore, the insula acts as a critical hub in this network. Evidence from intracranial EEG (iEEG) indicates its involvement in automatic deviance detection[37,72] and its role in coordinating hierarchical processing across sensory and salience networks[73].

In summary, the ASTM trace is processed through a precisely positioned hierarchical network. The initial, pre-attentive stages involve feedforward signaling of prediction error from lower sensory areas. This is followed by feedback interactions, where frontal regions modulate activity in the hippocampus and other temporal areas, facilitating the updating of

the short-term auditory model or context[66]. This comprehensive network model, revealed through direct intracranial recordings and connectivity analysis, offers a detailed framework for understanding how distributed brain regions, including the hippocampus, interact to form and maintain auditory short-term memory traces.

References

1. Bird CM, Burgess N. The hippocampus and memory: insights from spatial processing. *Nature reviews neuroscience* **9**, 182-194 (2008).
2. Husain M. The human hippocampus contributes to short-term memory. *Brain : a journal of neurology* **147**, 2593-2594 (2024).
3. Warrington EK. Amnesia and the distinction between long-and short-term memory. *Journal of verbal learning and verbal behavior* **9**, 176-189 (1970).
4. Cave CB, Squire LR. Intact verbal and nonverbal short-term memory following damage to the human hippocampus. *Hippocampus* **2**, 151-163 (1992).
5. Corkin S. Acquisition of Motor Skill after Bilateral Medial Temporal-Lobe Excision. *Neuropsychologia* **6**, 255-& (1968).
6. Moscovitch M. Recovered Consciousness - a Hypothesis Concerning Modularity and Episodic Memory. *Journal of Clinical and Experimental Neuropsychology* **17**, 276-290 (1995).
7. Squire LR. Memory and the hippocampus: a synthesis from findings with rats, monkeys, and humans. *Psychological review* **99**, 195-231 (1992).
8. Schacter DL. Implicit Memory: History and Current Status. *Journal of Experimental Psychology Learning Memory & Cognition* **13**, 501-518 (1987).
9. Cohen NJ, Squire LR. Preserved learning and retention of pattern-analyzing skill in amnesia: Dissociation of knowing how and knowing that. *Science* **210**, 207-210 (1980).
10. Steinvorth S, Levine B, Corkin S. Medial temporal lobe structures are needed to re-experience remote autobiographical memories: evidence from HM and WR. *Neuropsychologia* **43**, 479-496 (2005).
11. Scoville WB, & Milner, B. . Loss of recent memory after bilateral hippocampallesions. *J Neurol Neurosurg Psychiat* **20**, (1957).
12. Reber PJ. The neural basis of implicit learning and memory: a review of neuropsychological and neuroimaging research. *Neuropsychologia* **51**, 2026-2042 (2013).
13. Tulving E. Episodic memory: From mind to brain. *Annual review of psychology* **53**, 1-25 (2002).
14. Hannula DE, Tranel D, Cohen NJ. The long and the short of it: relational memory impairments in amnesia, even at short lags. *Journal of Neuroscience* **26**, 8352-8359 (2006).
15. Olson IR, Page K, Moore KS, Chatterjee A, Verfaellie M. Working memory for conjunctions relies on the medial temporal lobe. *Journal of Neuroscience* **26**, 4596-4601 (2006).
16. Daume J, *et al.* Control of working memory by phase–amplitude coupling of human hippocampal neurons. *Nature* **629**, 393-401 (2024).

17. Griffiths TD, *et al.* Cross-frequency coupling in cortico-hippocampal networks supports the maintenance of sequential auditory information in short-term memory. *PLOS Biology* **22**, (2024).

18. Cascella M, Al Khalili Y. Short-term memory impairment. In: *StatPearls [Internet]*). StatPearls Publishing (2024).

19. Näätänen RN, Paavilainen P, Rinne T, Alho K. The mismatch negativity (MMN) in basic research of central auditory processing: a review. *Clinical neurophysiology : official journal of the International Federation of Clinical Neurophysiology* **118**, 2544-2590 (2007).

20. Partanen E, Kujala T, Naatanen R, Liitola A, Sambeth A, Huotilainen M. Learning-induced neural plasticity of speech processing before birth. *Proceedings of the National Academy of Sciences of the United States of America* **110**, 15145-15150 (2013).

21. Colin C, Radeau M, Soquet A, Demolin D, Colin F, Deltenre P. Mismatch negativity evoked by the McGurk-MacDonald effect: a phonetic representation within short-term memory. *Clinical Neurophysiology* **113**, 495-506 (2002).

22. Näätänen R, Gaillard AWK, Mäntysalo S. Early Selective-Antention Effect on Evoked Potential Reinterpreted. *Acta Psychologica* **42**, 313-329 (1978).

23. Novak GP, Ritter W, Vaughan Jr HG, Wiznitzer ML. Differentiation of negative event-related potentials in an auditory discrimination task. *Electroencephalography and clinical neurophysiology* **75**, 255-275 (1990).

24. Näätänen R. The role of attention in auditory information processing as revealed by event-related potentials and other brain measures of cognitive function. *Behavioral and brain sciences* **13**, 201-233 (1990).

25. Cowan N, Winkler I, Teder W, Näätänen R. Memory prerequisites of mismatch negativity in the auditory event-related potential (ERP). *Journal of experimental psychology: Learning, Memory, and Cognition* **19**, 909 (1993).

26. Näätänen R, Alho K. Mismatch negativity-a unique measure of sensory processing in audition. *International Journal of Neuroscience* **80**, 317-337 (1995).

27. Teichert T, Jedema H, Zhen Z, Gurnsey K. Complementary functional profiles of mismatch responses mediated by adaptation and deviance detection point to two distinct auditory short-term memory systems. *Journal of neurophysiology* **134**, 314-336 (2025).

28. Tuomainen OT. Auditory short-term memory trace formation for nonspeech and speech in SLI and dyslexia as indexed by the N100 and mismatch negativity electrophysiological responses. *Neuroreport* **26**, 374-379 (2015).

29. Ray S, Maunsell JH. Different origins of gamma rhythm and high-gamma activity in macaque visual cortex. *PLoS Biol* **9**, e1000610 (2011).

30. Lachaux JP, Axmacher N, Mormann F, Halgren E, Crone NE. High-frequency neural activity and human cognition: past, present and possible future of intracranial EEG research. *Prog Neurobiol* **98**, 279-301 (2012).

31. Rich EL, Wallis JD. Spatiotemporal dynamics of information encoding revealed in orbitofrontal high-gamma. *Nature communications* **8**, 1139 (2017).

32. Watson BO, Ding M, Buzsaki G. Temporal coupling of field potentials and action potentials in the neocortex. *The European journal of neuroscience* **48**, 2482-2497 (2018).

33. Oostenveld R, Fries P, Maris E, Schoffelen JM. FieldTrip: Open source software for advanced analysis of MEG, EEG, and invasive electrophysiological data. *Comput Intell Neurosci* **2011**, 156869 (2011).

34. Stolk A, *et al*. Integrated analysis of anatomical and electrophysiological human intracranial data. *Nat Protoc* **13**, 1699-1723 (2018).

35. Studholme C, Hill DLG, Hawkes DJ. An overlap invariant entropy measure of 3D medical image alignment. *Pattern Recognition* **32**, 71-86 (1999).

36. Ashburner J, Friston KJ. Unified segmentation. *NeuroImage* **26**, 839-851 (2005).

37. Blenkmann AO, *et al*. Auditory deviance detection in the human insula: An intracranial EEG study. *Cortex* **121**, 189-200 (2019).

38. Mesgarani N, Cheung C, Johnson K, Chang EF. Phonetic Feature Encoding in Human Superior Temporal Gyrus. *Science* **343**, 1006-1010 (2014).

39. Norman Y, Yeagle EM, Harel M, Mehta AD, Malach R. Neuronal baseline shifts underlying boundary setting during free recall. *Nature Communications* **8**, 1301 (2017).

40. Smith SM, Nichols TE. Threshold-free cluster enhancement: Addressing problems of smoothing, threshold dependence and localisation in cluster inference. *NeuroImage* **44**, 83-98 (2009).

41. Winkler AM, Ridgway GR, Webster MA, Smith SM, Nichols TE. Permutation inference for the general linear model. *NeuroImage* **92**, 381-397 (2014).

42. Luck SJ. Event-related potentials from the user's perspective. *Nature neuroscience* **9**, 463 (2006).

43. Granger CWJ. Investigating causal relations by econometric models and cross-spectral methods. *Econometrica* **37**, 424-438 (1969).

44. Seth AK, Barrett AB, Barnett L. Granger Causality Analysis in Neuroscience and Neuroimaging. *Journal of Neuroscience* **35**, 3293-3297 (2015).

45. Bressler SL, Seth AK. Wiener-Granger causality: a well established methodology. *NeuroImage* **58**, 323-329 (2011).

46. Schreiber T. Measuring information transfer. *Physical review letters* **85**, 461 (2000).

47. Barnett L, Seth AK. The MVGC multivariate Granger causality toolbox: A new approach to Granger-causal inference. *Journal of Neuroscience Methods* **223**, 50-68 (2014).

48. Barnett L, Barrett AB, Seth AK. Granger causality and transfer entropy are equivalent for Gaussian variables. *Phys Rev Lett* **103**, 238701 (2009).

49. Barnett L, Seth AK. The MVGC multivariate Granger causality toolbox: a new approach to Granger-causal inference. *J Neurosci Methods* **223**, 50-68 (2014).

50. Seth AK. A MATLAB toolbox for Granger causal connectivity analysis. *J Neurosci Methods* **186**, 262-273 (2010).

51. Barnett L, Seth AK. Granger causality for state-space models. *Physical review E, Statistical, nonlinear, and soft matter physics* **91**, 040101 (2015).

52. Bouton ME, Bolles RC. Conditioned Fear Assessed by Freezing and by the Suppression of 3 Different Baselines. *Anim Learn Behav* **8**, 429-434 (1980).

53. Liberman T, Velluti RA, Pedemonte M. Temporal correlation between auditory neurons and the hippocampal theta rhythm induced by novel stimulations in awake guinea pigs. *Brain research* **1298**, 69-77 (2009).

54. Graham KS, Barense MD, Lee ACH. Going beyond LTM in the MTL: A synthesis of neuropsychological and neuroimaging findings on the role of the medial temporal lobe in memory and perception. *Neuropsychologia* **48**, 831-853 (2010).

55. Lee ACH, Yeung LK, Barense MD. The hippocampus and visual perception. *Frontiers in human neuroscience* **6**, (2012).

56. Lachaux JP, *et al.* The many faces of the gamma band response to complex visual stimuli. *NeuroImage* **25**, 491-501 (2005).

57. Lachaux JP, *et al.* Silence is golden: transient neural deactivation in the prefrontal cortex during attentive reading. *Cerebral cortex* **18**, 443-450 (2008).

58. Lachaux J-P, Axmacher N, Mormann F, Halgren E, Crone NE. High-frequency neural activity and human cognition: Past, present and possible future of intracranial EEG research. *Progress in neurobiology* **98**, 279-301 (2012).

59. Eckert D, *et al.* Distinct interacting cortical networks for stimulus-response and repetition-suppression. *Communications biology* **5**, 909 (2022).

60. Ishishita Y, *et al.* Deviance detection is the dominant component of auditory contextual processing in the lateral superior temporal gyrus: A human ECoG study. *Human brain mapping* **40**, 1184-1194 (2019).

61. Mehta AD, *et al.* Seizure propagation in a patient with musicogenic epilepsy. *Epilepsy & Behavior* **14**, 421-424 (2009).

62. Chatani H, *et al.* Neuromagnetic evidence for hippocampal modulation of auditory processing. *NeuroImage* **124**, 256-266 (2016).

63. Xiao C, Liu Y, Xu J, Gan X, Xiao Z. Septal and Hippocampal Neurons Contribute to Auditory Relay and Fear Conditioning. *Frontiers in cellular neuroscience* **12**, 102 (2018).

64. Nishitani N, *et al.* The role of the hippocampus in auditory processing studied by event-related electric potentials and magnetic fields in epilepsy patients before and after temporal lobectomy. *Brain : a journal of neurology* **122 (Pt 4)**, 687-707 (1999).

65. Garrido MI, Barnes GR, Kumaran D, Maguire EA, Dolan RJ. Ventromedial prefrontal cortex drives hippocampal theta oscillations induced by mismatch computations. *NeuroImage* **120**, 362-370 (2015).

66. Fonken YM, Kam JWY, Knight RT. A differential role for human hippocampus in novelty and contextual processing: Implications for P300. *Psychophysiology* **57**, (2019).

67. Durschmid S, *et al.* Hierarchy of prediction errors for auditory events in human temporal and frontal cortex. *Proceedings of the National Academy of Sciences of the United States of America* **113**, 6755-6760 (2016).

68. Hsu YF, Le Bars S, Hamalainen JA, Waszak F. Distinctive Representation of Mispredicted and Unpredicted Prediction Errors in Human Electroencephalography. *The Journal of neuroscience : the official journal of the Society for Neuroscience* **35**, 14653-14660 (2015).

69. Recasens M, Gross J, Uhlhaas PJ. Low-Frequency Oscillatory Correlates of Auditory Predictive Processing in Cortical-Subcortical Networks: A MEG-Study. *Sci Rep-Uk* **8**, (2018).

70. Naatanen R, Gaillard AW, Mantysalo S. Early selective-attention effect on evoked potential reinterpreted. *Acta Psychol (Amst)* **42**, 313-329 (1978).

71. Oestreich LKL, Randeniya R, Garrido MI. Auditory white matter pathways are associated with effective connectivity of auditory prediction errors within a fronto-temporal network. *NeuroImage* **195**, 454-462 (2019).

72. Zhang Y, *et al.* The Roles of Subdivisions of Human Insula in Emotion Perception and Auditory Processing. *Cerebral cortex* **29**, 517-528 (2019).

73. Allen M, *et al.* Anterior insula coordinates hierarchical processing of tactile mismatch responses. *NeuroImage* **127**, 34-43 (2016).

Figure legends

Fig. 1 Experimental design and channel localizations. Experiment design and channel localizations. a Auditory oddball paradigm: Stimuli consisted of 300 ms pure tones (including 10 ms fade-in and fade-out periods). The standard tone (500 Hz) accounted for 90% of trials, while the deviant tone (700 Hz) comprised the remaining 10%. **b** 3D reconstruction of the brain with implanted electrodes showing significant responses. To improve clarity, non-responsive electrode shafts are omitted. Small black dots represent channels without significant responses; large colored dots indicate channels with significant responses, with each color corresponding to a different subject.

Fig. 2 Hippocampal high-frequency activity (HFA) responses to pure tones.

a Averaged positive HFA responses to elicited by standard stimuli. **b** Heatmap of a single exemplar channel from the group presented in **a**. **c** Averaged negative HFA responses (or high-frequency suppression) elicited by standard stimuli, **d** Heatmap of a single exemplar channel from the group presented in **c**. **e** Averaged positive HFA responses to elicited by deviant stimuli. **f** Heatmap of a single exemplar channel from the group presented in **e**. **g** Averaged negative HFA responses (or high-frequency suppression) elicited by deviant stimuli. **h** Heatmap of a single exemplar channel from the group presented in **g**. In panels **a**,

c, **e**, **g**, blue lines denote responses to standard trials; red lines represent responses to deviant trials. Shaded areas indicate mean ± SEM. n indicates the number of channels averaged, and s indicates the number of subjects. In panels **b**, **d**, **f**, **h**, yellow traces represent positive HFA responses; blue traces indicate negative HFA responses high-frequency suppression (or high-frequency suppression). Solid black vertical line indicates the onset of the stimulus, dashed lines indicate the time windows exhibiting statistically significant responses to auditory stimuli ($p < 0.05$).

Fig. 3 Classification of mean HFA responses to pure tones. Responses were averaged across channels from different subjects showing significant differences between the deviant and standard conditions. Mean HFA and high frequency suppression (HFS) responses are shown for standard (blue dashed line) and deviant tones (red dashed line), along with deviant-minus-standard difference waveforms (green solid line). **a** Mean HFS responses to standard and deviant pure tones. **b** Mean HFA responses to standard and deviant pure tones. **c** Mean HFA responses with no response to standard pure tones. **d** Mean HFA responses with significant responses to standard pure tones ($p < 0.05$). Shadowed areas depict mean ± SEM, n indicates the number of channels averaged, and s indicates the number of subjects.

Fig. 4 Latencies of HFA responses in different brain regions and Granger causality analysis of brain connectivity within different brain regions. a Mean HFA/HFS responses to standard (blue dash line) and deviant pure tones (red dash line), as well as deviant-minus-standard difference waveforms (green solid line), are plotted for the insula, temporal lobe (including Heschl's gyrus, superior temporal gyrus, superior temporal sulcus), frontal lobe (including the middle frontal gyrus, superior frontal gyrus, anterior cingulate cortex, frontal operculum), parietal lobe (including postcentral gyrus, parietal operculum, supramaginal gyrus), posterior temporal lobe (including temporo-occipital partition in the middle temporal gyrus), inferior temporal lobe (including inferior temporal gyrus, fusiform gyrus, and inferior of middle temporal gyrus) and the hippocampus area (including hippocampus, parahippocampal gyrus, amygdala). n indicates the number of channels averaged, and s indicates the number of subjects. **b** The scatter plot shows the response latencies of HFA/HFS in the electrode pairs from the brain regions mentioned above. The blue line indicates the ascending trend of the latencies of different brain areas. **c** The heatmap shows the

connectivity between these brain regions. Estimates of the difference in Granger causal connection strengths between deviant and standard stimulus-evoked activity across brain regions. Each position in the plot indicates the strength of connections corresponding from the row to the column. Gray indicates no significant difference, and color indicates significant connection within brain areas. Specific brain regions calculated included in this figure are shown as follows. The insula; temporal lobe: including Heschl's gyrus, superior temporal gyrus, superior temporal sulcus; frontal lobe: including the middle frontal gyrus, superior frontal gyrus, anterior cingulate cortex, frontal operculum; parietal lobe: including postcentral gyrus, parietal operculum, supramaginal gyrus; posterior temporal lobe: including temporo-occipital part in the middle temporal gyrus: inferior temporal lobe: including inferior temporal gyrus, fusiform gyrus, and inferior of middle temporal gyrus; and the hippocampus area: including hippocampus, parahippocampal gyrus, amygdala.

Fig. 5 Granger causality-based connectivity across brain regions.

Anatomical locations of regions identified by Granger causality analysis are projected onto a common cortical surface. The enlarged inset highlights the boxed area. Distinct colors represent different functional clusters and the directionality of connections (bottom-up vs. top-down) within these regions.

Supplementary Fig. 1 HFA responses to different pure tones of Sub 3. HFA of tone-responsive channels evoked by standard (blue lines) and deviant (red lines) pure tones are plotted for sub 3, shadowed areas depict mean ± SEM. The latencies of HFA at each channel were shown in each plot. Significant effects are marked at the top image, gray indicates there is no significant difference between response to standard and deviant stimuli, and color indicates significant deviance detection.

Supplementary Fig. 2 Mean ERP responses to different pure tones. ERP responses were averaged across channels from different subjects showing significant differences between the deviant and standard conditions. Only channels that showed significant responses to both conditions within each dimension of analysis were included in the plots in order to obtain comparable waveforms. **a** Responses for Group 1. **b** Responses for Group 2. **c** Responses for Group 3. **d** Responses for Group 4. Mean ERP responses to standard (blue dash line) and

deviant pure tones (red dash line), as well as deviant-minus-standard difference waveforms (green solid line), are plotted for subjects. Shadowed areas depict mean ± SEM, n indicates the number of channels averaged, and s indicates the number of subjects.

Supplementary Fig. 3 Mean ERP responses to different pure tones. ERP responses were averaged across channels from different subjects showing significant differences between the deviant and standard conditions. Only channels that showed significant responses to both conditions within each dimension of analysis were included in the plots in order to obtain comparable waveforms. (A) Responses for Group 1. (B) Responses for Group 2. (C) Responses for Group 3. d Responses for Group 4. Mean ERP responses to standard (blue dash line) and deviant pure tones (red dash line), as well as deviant-minus-standard difference waveforms (green solid line), are plotted for subjects. Shadowed areas depict mean ± SEM, n indicates the number of channels averaged, and s indicates the number of subjects.

Figure 1

a

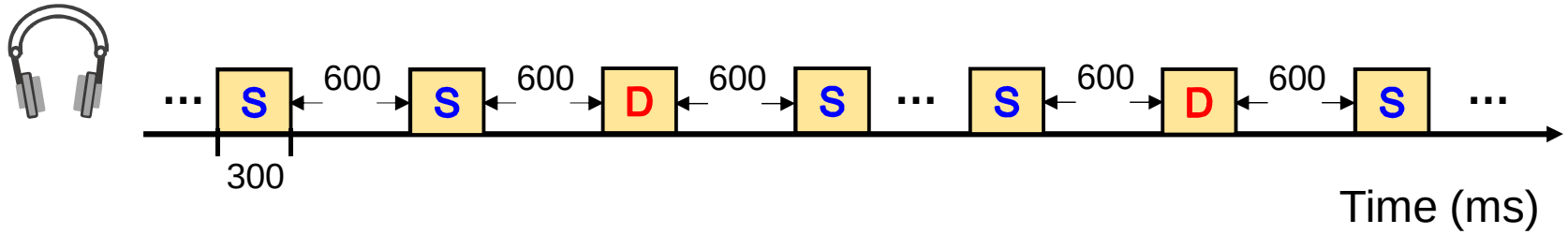

b

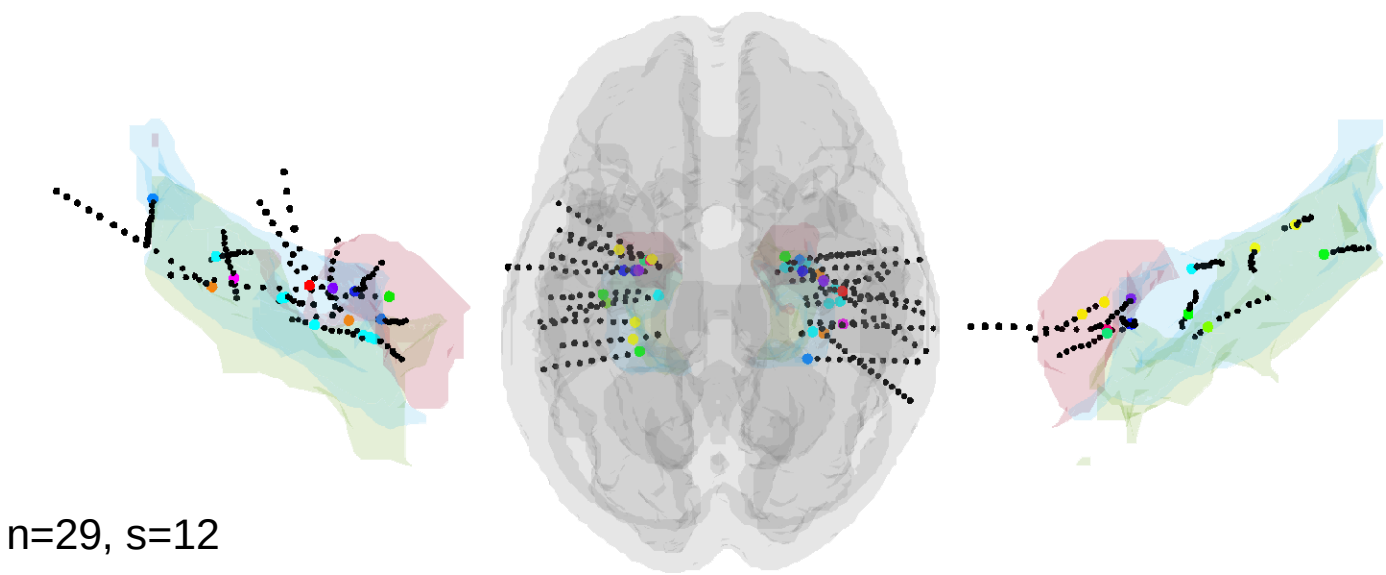

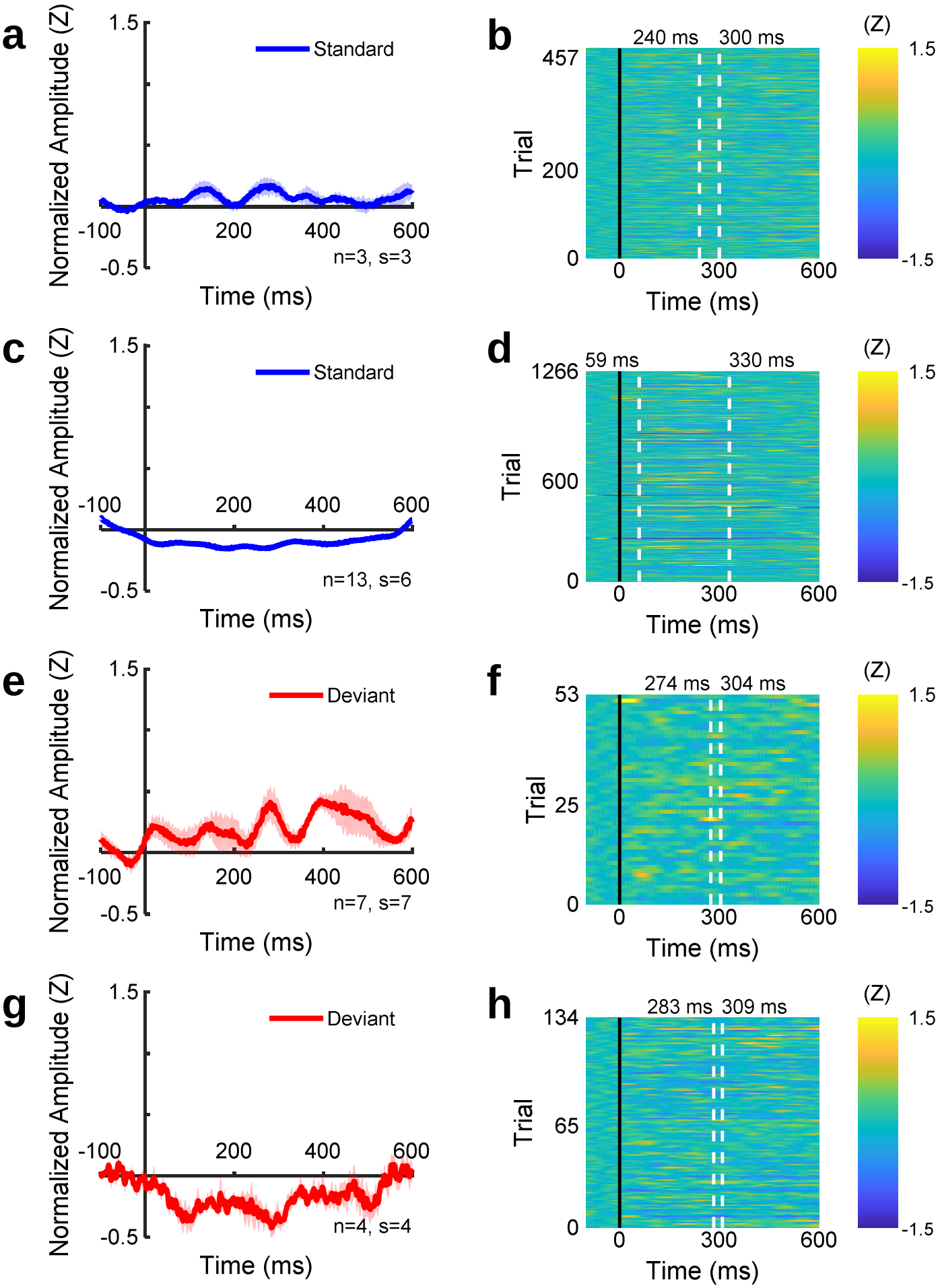
a
Standard
Normalized Amplitude (Z)
1.5
-0.5
-100
200
400
600
n=3, s=3
Time (ms)
b
240 ms
300 ms
457
200
0
Trial
0
300
600
Time (ms)
(Z)
1.5
-1.5
c
Standard
Normalized Amplitude (Z)
1.5
-0.5
-100
200
400
600
n=13, s=6
Time (ms)
d
59 ms
330 ms
1266
600
0
Trial
0
300
600
Time (ms)
(Z)
1.5
-1.5
e
Deviant
Normalized Amplitude (Z)
1.5
-0.5
-100
200
400
600
n=7, s=7
Time (ms)
f
274 ms
304 ms
53
25
0
Trial
0
300
600
Time (ms)
(Z)
1.5
-1.5
g
Deviant
Normalized Amplitude (Z)
1.5
-0.5
-100
200
400
600
n=4, s=4
Time (ms)
h
283 ms
309 ms
134
65
0
Trial
0
300
600
Time (ms)
(Z)
1.5
-1.5

Figure 3

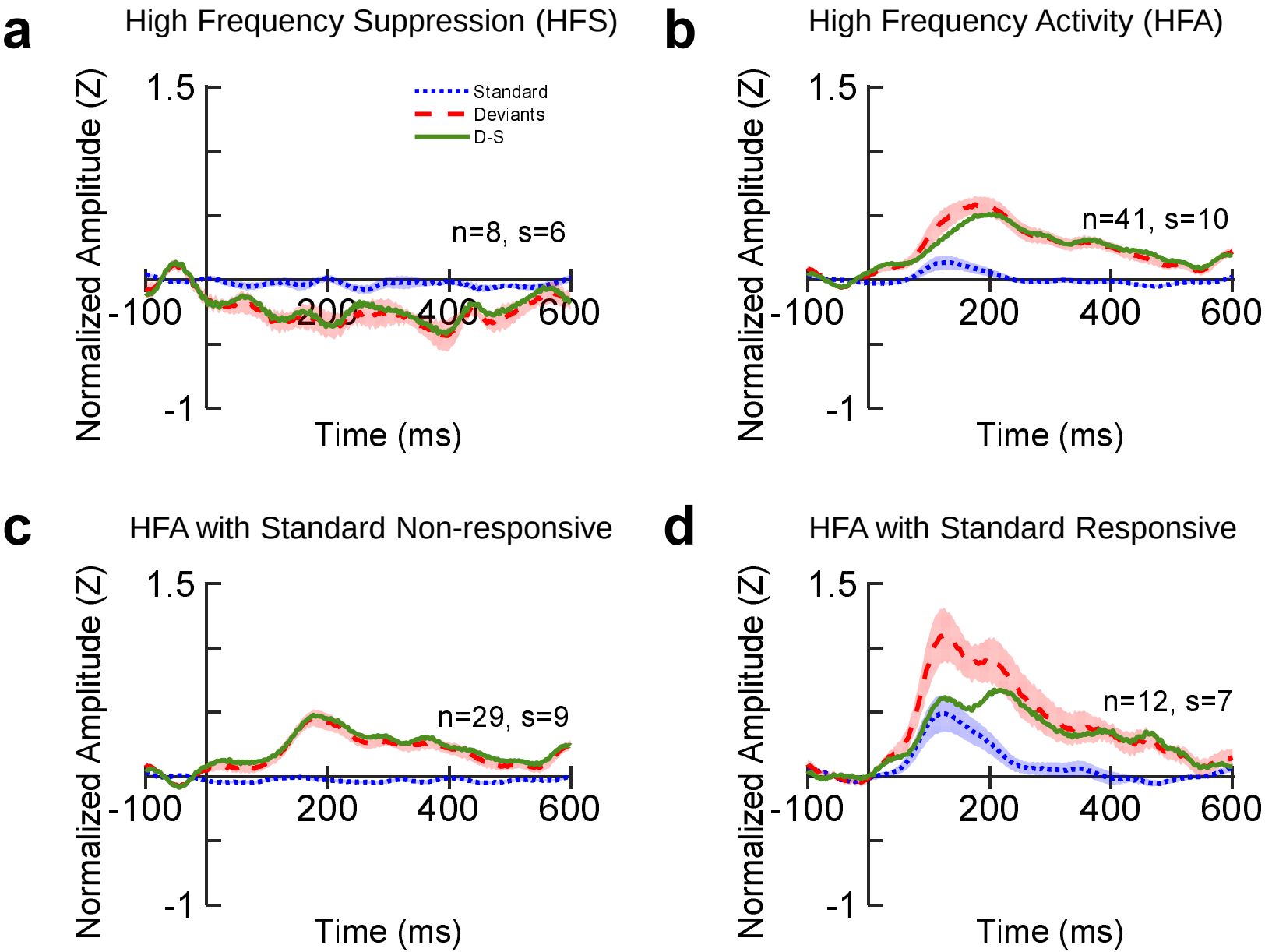
a
High Frequency Suppression (HFS)
Standard
Deviants
D-S
n=8, s=6
Normalized Amplitude (Z)
1.5
-1
-100
200
400
600
Time (ms)
b
High Frequency Activity (HFA)
n=41, s=10
Normalized Amplitude (Z)
1.5
-1
-100
200
400
600
Time (ms)
c
HFA with Standard Non-responsive
n=29, s=9
Normalized Amplitude (Z)
1.5
-1
-100
200
400
600
Time (ms)
d
HFA with Standard Responsive
n=12, s=7
Normalized Amplitude (Z)
1.5
-1
-100
200
400
600
Time (ms)

Figure 4

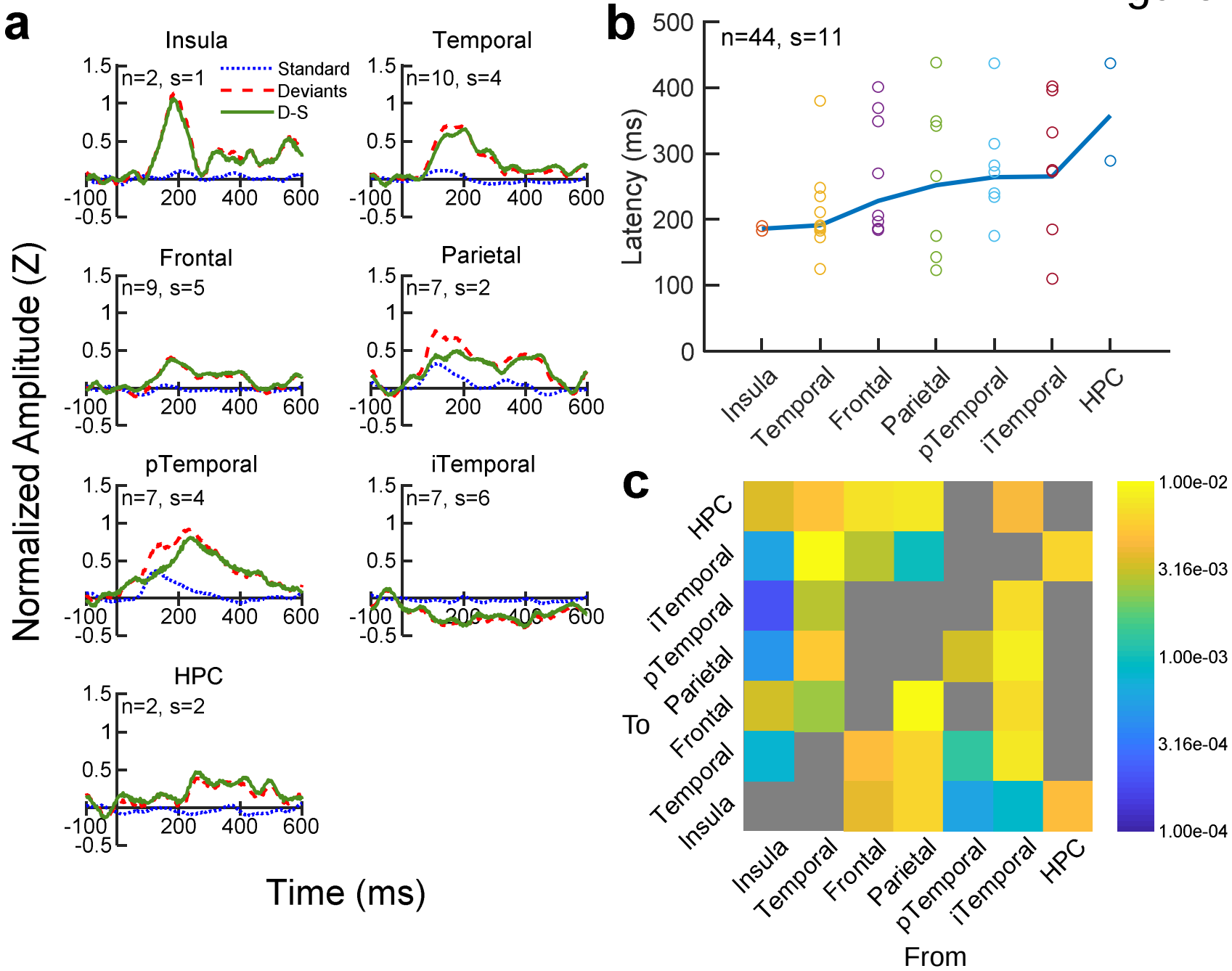
a
Insula
n=2, s=1
Standard
Deviants
D-S
Temporal
n=10, s=4
Frontal
n=9, s=5
Parietal
n=7, s=2
pTemporal
n=7, s=4
iTemporal
n=7, s=6
HPC
n=2, s=2
Normalized Amplitude (Z)
Time (ms)
b
n=44, s=11
Latency (ms)
Insula
Temporal
Frontal
Parietal
pTemporal
iTemporal
HPC
c
To
From
1.00e-02
3.16e-03
1.00e-03
3.16e-04
1.00e-04

Figure 5

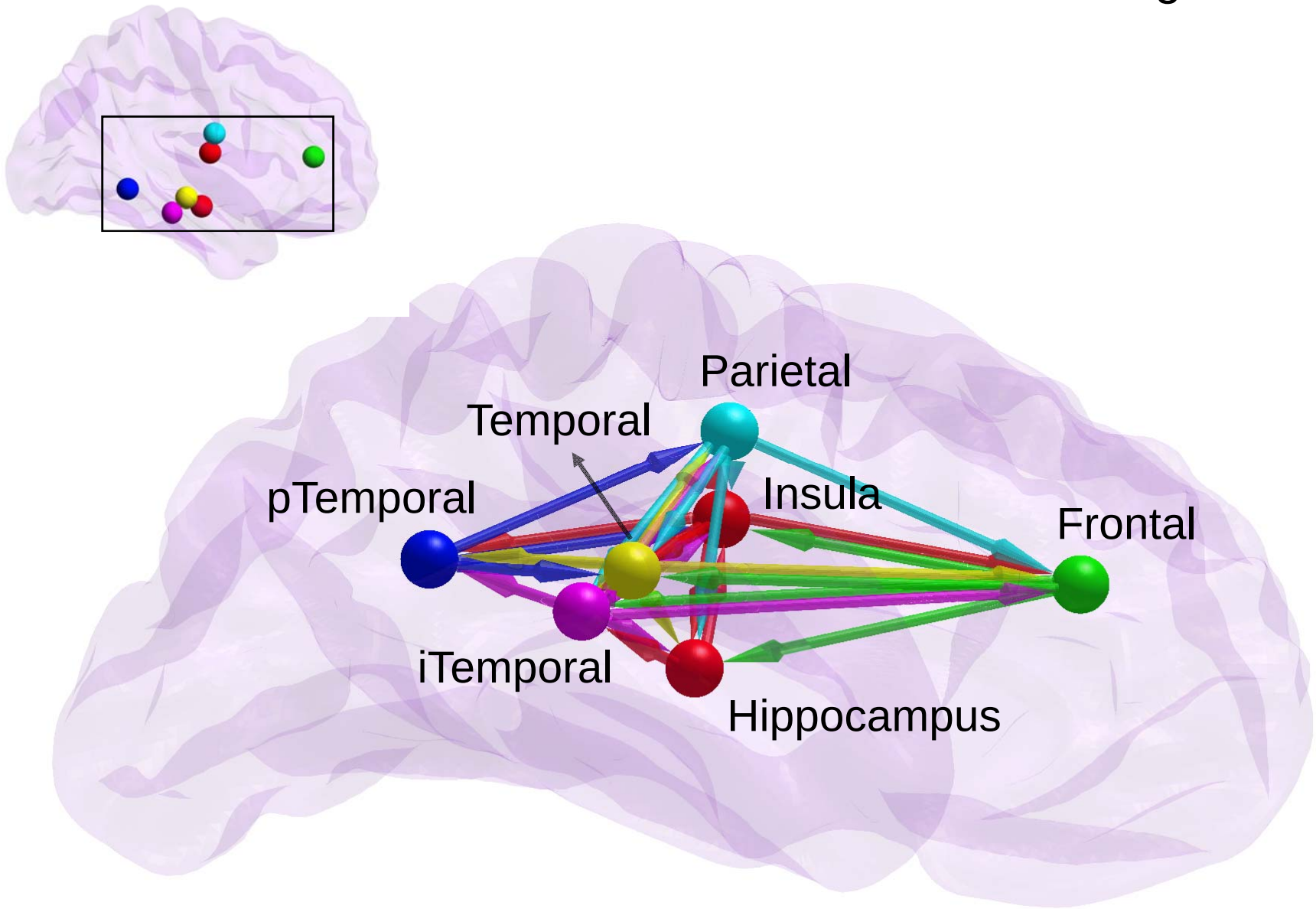
Parietal
Temporal
pTemporal
Insula
Frontal
iTemporal
Hippocampus

Supplementary Figure 1

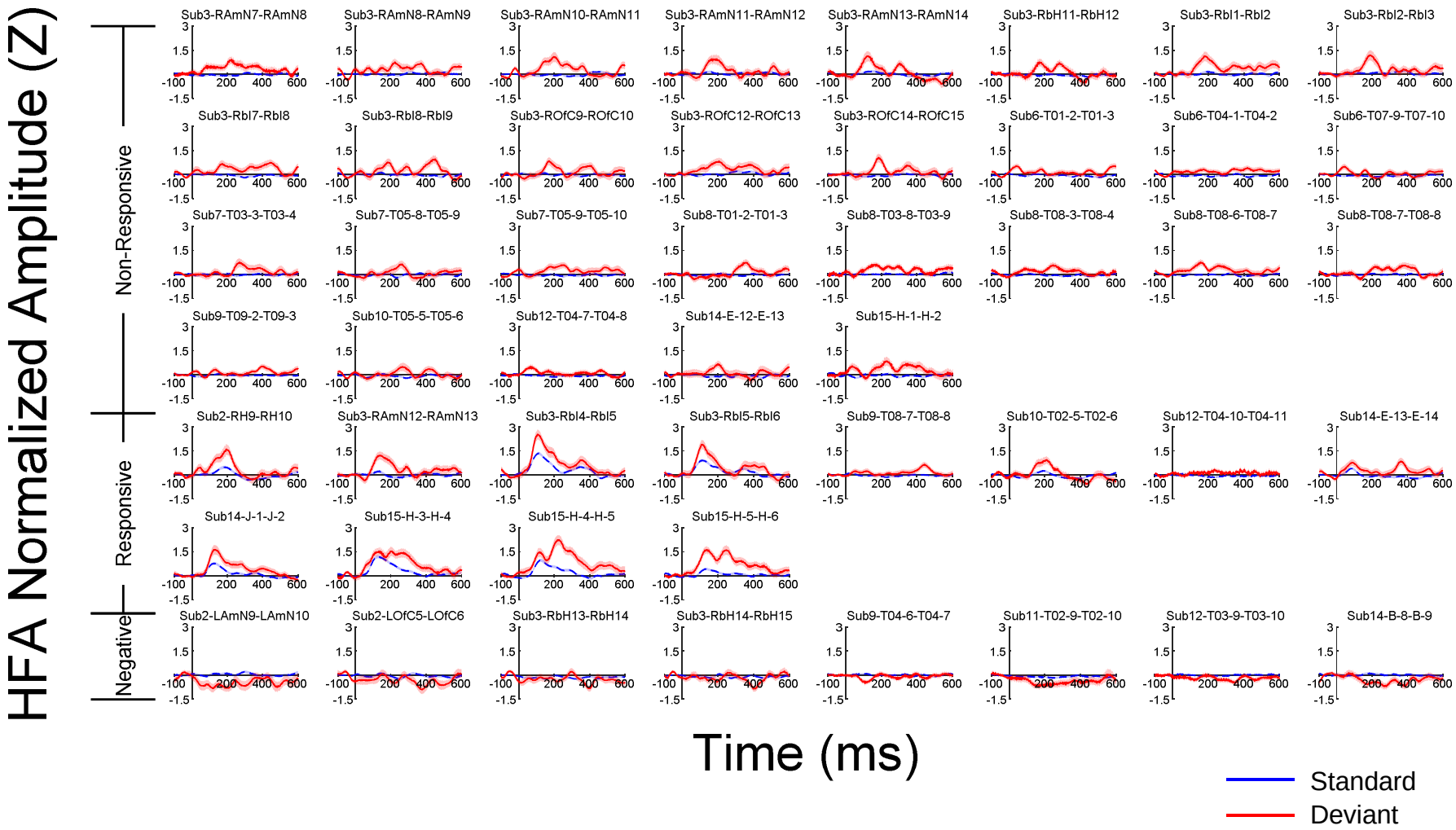

Supplementary Figure 2

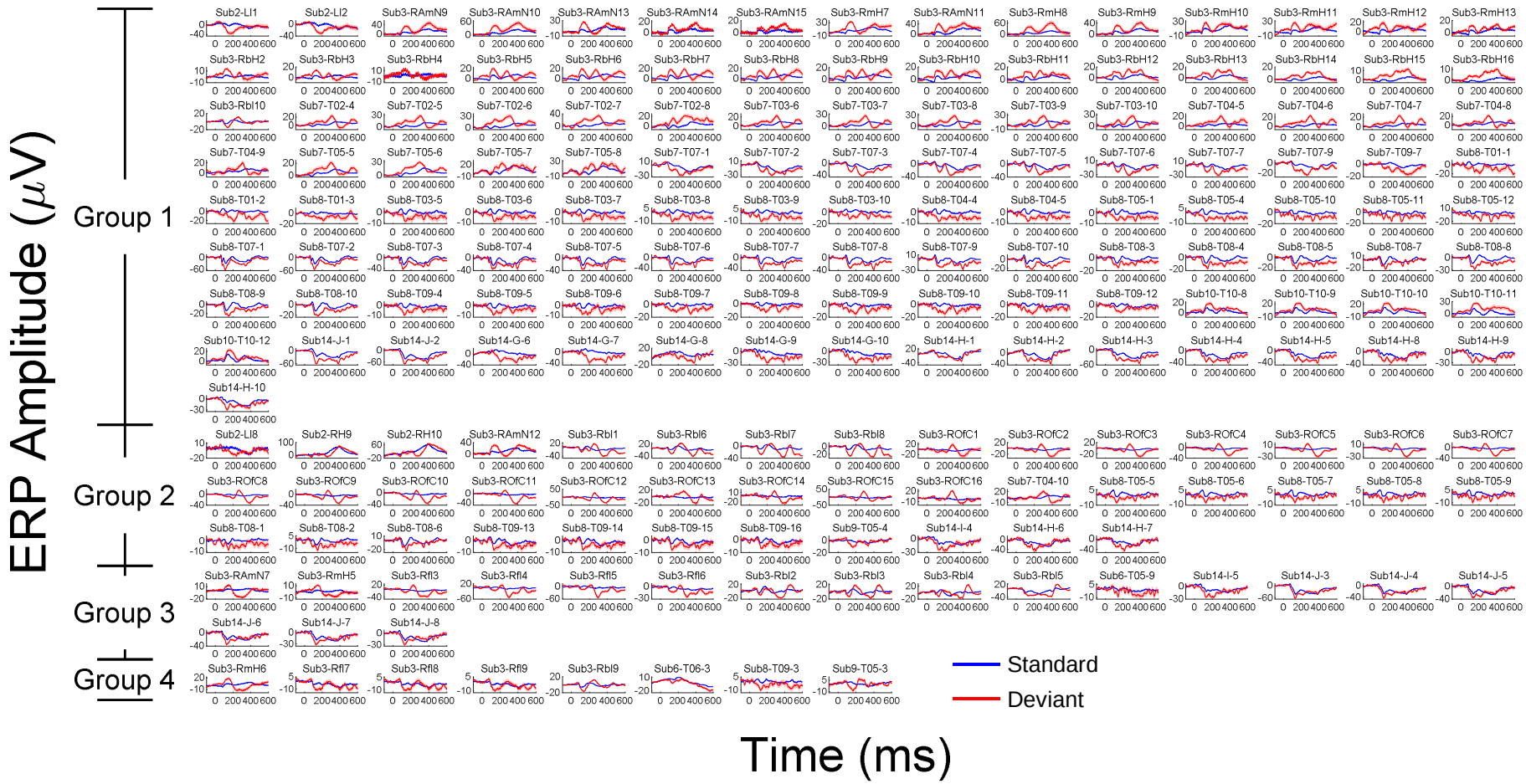
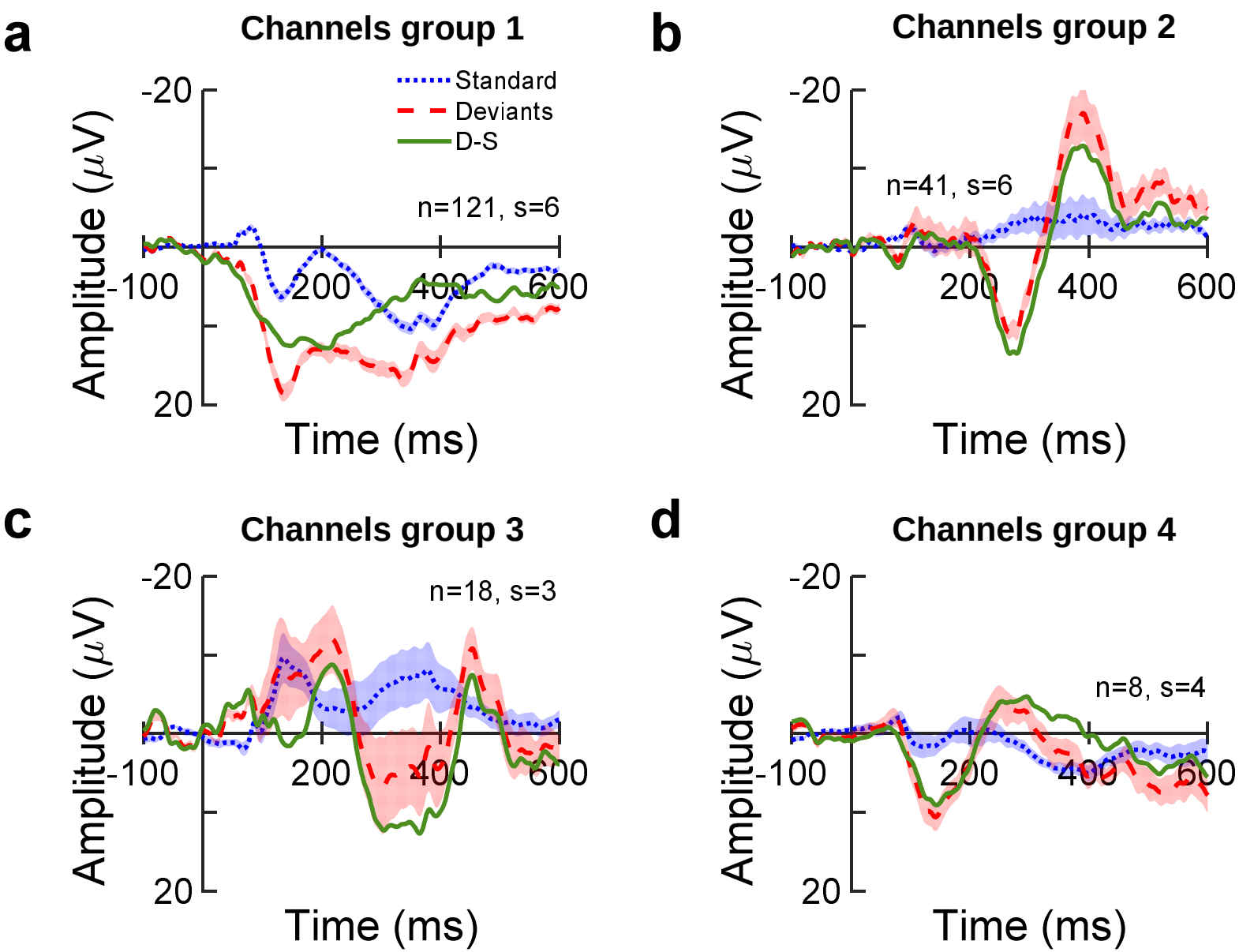
Supplementary Figure 3